RSC Advances

PAPER

View Article Online
View Journal | View Issue

Cite this: *RSC Adv.*, 2024, **14**, 34156

Low temperature synthesis of franklinite stabilized cefixime as a multifunctional nanoformulation

Amna Munsaf,[ab] Muhammad Naeem Ahmed,[*a] Aroosa Zafar,[c] Bilal Akram[*bd] and Mahmoud A. A. Ibrahim[ef]

Cefixime, an antibiotic with low solubility, stability, bioavailability and therapeutic effectiveness, needs to be administered in larger doses for effective treatment. This can lead to higher healthcare costs and increased risk of side effects, negatively affecting public health. Herein, we aim to develop a strategy to overcome the aforementioned limitations by stabilizing it using franklinite nanostructures. Franklinite nanostructures ($ZnFe_2O_4$) were synthesized *via* a green method and subsequently used as a support to stabilize cefixime (Cef). The successful formation of $ZnFe_2O_4$ nanostructures and subsequent loading of the drug was confirmed using various microscopic and spectroscopic analyses. Solubility measurements and dissolution tests for the franklinite stabilized cefixime (Cef–$ZnFe_2O_4$) indicated increased solubility, enhanced *in vitro* bioavailability and greater absorption under physiological conditions. Hemolytic assay affirmed the safety and efficacy of drug stabilized by franklinite. Biological assessment of Cef–$ZnFe_2O_4$ revealed that it has strong antifungal, antioxidant and kinase inhibition potential as compared to its bare counterpart. These findings emphasize the potential of newly designed Cef–$ZnFe_2O_4$ as a promising nanoformulation with enhanced solubility, efficacy, safety and biological activities.

Received 6th September 2024
Accepted 12th October 2024

DOI: 10.1039/d4ra06435f

rsc.li/rsc-advances

Introduction

Traditional medications, despite their clinical applications, often face limitations in optimizing their therapeutic efficacy while minimizing associated side effects. These limitations include low bioavailability, less solubility and emergence of antimicrobial resistance. These issues demand high drug doses to achieve the desired effect, leading to increased side effects, reduced adherence and rapid excretion from the body.[1,2] Cefixime is a broad-spectrum cephalosporin antibiotic characterized by poor solubility and instability under certain conditions. These properties restrict its absorption in the gastrointestinal tract and consequently diminish its therapeutic effectiveness.[3,4] Furthermore, these limitations can result in less-than-ideal therapeutic outcomes and contribute to the development of antibiotic resistance.

To address these concerns, nanotechnology has opened a path to advanced treatment strategies through nanomedicines.[5] The scientific community has been recently showing increasing interest in nanomaterials owing to the combined physicochemical characteristics of their constituent parts.[6–8] These nanomaterials hold significant importance across various scientific and technological fields, including optics, electronics, environmental science, aerospace[9,10] and medicine, due to their diverse applications, which are influenced by their structures, compositions and stabilities.[11,12] Metal oxide-based nanomaterials, owing to their inherent properties, have been reported as promising solutions for addressing a range of ailments, including microbial infections,[13] inflammations,[14] malignancies[15] and liver disorders.[16–20] Due to their biocompatibility, chemical stability, ease of separation and cost-effectiveness, they are ideal for biomedical applications.[21–23] By incorporating therapeutic agents into nanoscale matrices, nanomaterials offer several advantages, including increased drug stability, solubility, bioavailability and efficacy.[24–28]

Transition metal ferrites possess versatile characteristics, such as high surface area, high chemical stability, high surface active sites, strong magnetic properties and ease of functionalization. These properties make them key components in a wide range of industrial and technological applications.[29] Franklinite, in particular, offers a unique combination of properties. The presence of both Fe and Zn atoms enhances the stability of franklinite nanostructures and imparts bi-functional

[a]*Department of Chemistry, The University of Azad Jammu & Kashmir, Muzaffarabad 13100, Pakistan*
[b]*Department of Chemistry, Women University of Azad Jammu & Kashmir, Bagh 12500, AJ&K, Pakistan*
[c]*Department of Pharmacy, Faculty of Biological Sciences, Quaid-i-Azam University, Islamabad 45320, Pakistan*
[d]*Department of Chemistry, Tsinghua University, Beijing, China*
[e]*Computational Chemistry Laboratory, Chemistry Department, Faculty of Science, Minia University, Minia 61519, Egypt*
[f]*School of Health Sciences, University of KwaZulu-Natal, Westville Campus, Durban 4000, South Africa*

properties, making them ideal for specialized applications.[30,31] In recent years, these nanostructures have gained growing attention for biomedical uses due to their physiological compatibility, biosafety and potential in targeted drug delivery.[32] Therefore, the combination of superior stability, magnetic properties, biosafety and potential for functionalization makes franklinite an excellent choice to stabilize cefixime for advanced biomedical applications.

The quest for an environmentally sustainable and revolutionary method to generate metal oxide-based nanocomposites is unceasing. Nanocomposites can be achieved through several methods, including the sol–gel process, pulse laser desorption, mechanical milling, spray pyrolysis, thermal evaporation and microwave-assisted techniques.[33] Unfortunately, these methods are highly expensive and involve the extensive use of toxic chemicals requiring a large workforce and posing dangers to the environment. Some hazardous chemicals used in chemical methods can have harmful effects in the medical field.[34] However, green synthesis using biowaste promotes a non-toxic, eco-friendly approach to nanomaterial synthesis.[35,36] Agricultural wastes contain abundant secondary metabolites that reduce the metal ions through enzymes, amino acids, phenolic compounds and vitamins, which act as natural reducing agents.[37] Additionally, this approach also lowers the synthesis costs and energy requirements as compared to physical and chemical methods.[38,39]

Current research seeks to examine the biological efficacy, solubility and biocompatibility of franklinite stabilized cefixime under various physiological conditions synthesized using *Buddleja asiatica* leaves. Through the fusion of green chemistry and nanocomposite innovation, our investigation aims to thoroughly evaluate the therapeutic capabilities of the composite. This assessment includes a range of *in vitro* assays such as antioxidant, hemolytic, antifungal and protein kinase inhibition assays offering a holistic understanding of its pharmacological potential.

Experimental

Materials and methods

Chemicals. Zinc acetate dihydrate ($Zn(CH_3COO)_2 \cdot 2H_2O$), ferric sulphate $Fe_2(SO4)_3$, ethanol (CH_3CH_2OH), 2,2-diphenyl-1-picryl hydrazyl (DPPH), trichloro acetic acid ($C_2HCl_3O_2$), iodine (I_2), methanol CH_3OH, nutrient agar, potassium ferricyanide ($K_3Fe(CN)_6$), potassium acetate (CH_3COOK), potassium iodide (KI), dimethyl sulfoxide (DMSO), potassium hydrogen phosphate (K_2HPO_4), sulphuric acid (H_2SO_4), sodium phosphate (Na_2HPO_4), ammonium molybdate $(NH_4)_2MoO_4$, and starch, were provided by Sigma-Aldrich and used as received without any additional purification. Dried instant yeast was purchased from Fermipan (Fermipan BDH, England). Tween 20 was purchased from Merck (Merck-Schuchardt, USA). Cefixime, surfactin-B and amphotericin B and Triton-X were purchased from Sigma (Sigma-Aldrich USA).

The chemicals used in the recent exploration were of analytical grade and were utilized as provided.

Strains and cultures. Fungal strains included in this study were, *Aspergillus fumigatus* (FCBP-66), *Aspergillus flavus* (FCBP-0064), *Aspergillus niger* (FCBP-0198) and *Mucor* species (FCBP-0300).

Instruments used. An incubator IC83 (Yamato Japan), microplate reader (Elx 800, Biotek, USA), centrifuge (B. Braun, Germany), light microscope (Irmeco Germany), culture inoculum, laminar air flow hood, Petri dishes, micropipette (Sartorius, France), sterile transparent 96 well plate (SPL Life Science, Korea), sonicator (Sweepzone Technology USA), hot plate, oven and muffle furnace. An X-ray diffractometer (Malvern Panalytical, MPD), UV-visible spectrophotometer (XB20), Fourier transform infrared (Bruker, ALPHA), transmission electron microscope (PHILIPS, CM 120 TEM), scanning electron microscope (TESCAN, MIRA III SEM), and energy dispersive X-ray techniques.

Prior to usage, glass wares were washed with a 5% nitric acid solution and rinsed twice with deionized water. All the solutions utilized in this study were prepared in deionized water.

Preparation of extract. Collected leaves of *B. asiatica* leaves were thoroughly washed with tap water twice and once with distilled water to remove dirt and debris. After that, they were air-dried and then ground to fine powder. This powder was mixed with distilled water and constantly stirred for half an hour at 80 °C temperature. The resulting brownish extract was then filtered and stored in a refrigerator for future experimental use.

Synthesis of franklinite ($ZnFe_2O_4$) nanostructures. A mixture was prepared by combining 50 ml of a 0.1 M zinc acetate dihydrate solution with 50 ml of 0.1 M iron sulphate solution. To this mixture, 50 ml of plant extract was added causing the initially orange-colored metallic salt solution to transform into a dark orange mixture. This mixture was then stirred continuously for 2 h at 80 °C and allowed to stand overnight at room temperature. The supernatant was discarded carefully the next day. The remaining suspension was then subjected to three wash cycles with distilled water and one with ethanol. Finally, the mixture was centrifuged at 3500 rpm for 20 minutes, and the obtained supernatant was discarded. Subsequently, the dark orange material obtained was dried at 90 °C in an oven and then calcined at 500 °C in a muffle furnace for 5 h. After meticulous collection, it was powdered using a pestle and mortar and stored for further investigation.

Cefixime loading. Following a slightly adjusted standard protocol[40] the process began by adjusting 0.3 g of cefixime in distilled water, which was then placed into a burette. In a parallel step, 1 g of synthesized material was mixed into distilled water to create a suspension, ultrasonically. This was followed by the gradual addition of the cefixime solution to the suspension maintaining constant heat and stirring for one hour. After this period the mixture was exposed to ultrasonic waves at room temperature for 10 min and was then left to stand, overnight. The next steps involved centrifugation of the mixture at 10 000 rpm for 10 minutes to separate the cefixime loaded composite, which was then washed double with distilled water and once with DMSO to get rid of the unloaded cefixime.

After the drying process, the drug loading efficiency was determined.

Characterization. Green synthesized bare as well as cefixime-stabilized $ZnFe_2O_4$ nanostructures were characterized using various instruments: X-ray diffraction (Malvern Panalytical, MPD) was used to determine the crystalline nature, UV-visible spectrophotometer (XB20) was used to reveal their optical properties, Fourier transform infrared (Bruker, ALPHA) was used to identify specific functional groups, and transmission electron microscopy (PHILIPS, CM 120 TEM) and scanning electron microscope (TESCAN, MIRA III SEM) were used to characterize their morphology. Energy dispersive X-ray (EDX) analysis confirmed elemental composition, providing a comprehensive understanding of their structure and properties.

Solubility studies of franklinite ($ZnFe_2O_4$) nanostructures. To evaluate the solubility, the dispersions of $ZnFe_2O_4$ nanostructures were prepared in a buffer solution with pH levels of 1.2 (stimulating stomach acidity), 4.5 (pH of upper intestine) and 7.4 (matching the pH of blood). These dispersions were separated into two batches, each subjected to a controlled temperature of 25 °C and 37 °C. After this, the samples were allowed to become thermally stable and then agitated for 24 h to reach the equilibrium. Following the period of agitation, the mixture was centrifuged to filter out to separate undissolved nanoparticles. The clear supernatant was then collected and the concentrated cefixime was measured using UV visible spectrophotometry against a calibration curve. Solubility for each set of pH and temperature conditions was thus determined.

***In vitro* bioavailability evaluation.** A dissolution test was carried out to determine the comparative *in vitro* bioavailability of raw cefixime and cefixime-stabilized franklinite (Cef–$ZnFe_2O_4$) nanostructures using a paddle apparatus (USP apparatus 2) at pH 7.4. An appropriate amount of each sample was dissolved in a small volume of dissolution medium Phosphate buffer saline (PBS) containing 0.5% of Tween 80. The apparatus was operated with the paddle spinning at 75 rpm in 900 ml of preheated and the dissolution medium PBS was degassed to prevent any air bubbles. The test began once the temperature reached 37 °C. Every 1–120 minutes, 5 ml samples were collected, and filtered through a 0.45 μm Millipore filter and the lost volume was replaced with the same temperature medium. Drug concentration in each sample was measured using a UV-visible spectrophotometer. Each data point is the average of three measurements and variability is presented as the standard deviation. The results were plotted to show the cumulative percentage of drugs released over time.

In vitro biocompatibility evaluation

Hemolytic assay. To assess the interaction of the green-synthesized $ZnFe_2O_4$ (bare and cefixime loaded) nanostructures with blood cells, the hemolytic assay was performed. Firstly, the blood from the human donor was collected and then mixed with EDTA to prevent clot formation. In each Eppendorf 1 ml of blood was added and centrifuged at 10 000 rpm for 10 min. The supernatant was removed, and 1 ml PBS was added to each Eppendorf tube and centrifuged to wash the blood cells. The supernatant was discarded, and the process was repeated three times. The PBS was added to the Eppendorf tube to make a 5% solution of cells. 150 μl of the sample was added to the Eppendorf tube, then 350 μl of blood cells were added to each Eppendorf tube. The Eppendorf tubes were incubated at 37 °C for 30 min and then centrifuged at 10 000 rpm for 5 min. 200 μl of supernatant was added to 96 well plates and absorbance was measured at 530 nm. The % age hemolytic activity was calculated by the formula,

$$\%\ \text{hemolysis} = A_s - A_n/A_p - A_n \times 100$$

where, A_s = absorbance of sample, A_n = absorbance of negative control, A_p = absorbance of positive control.

Protein kinase inhibition assay. The protein kinase inhibitory potential of the test compounds was determined using the strain of *Streptomyces* 85E. For 24 hours, the *Streptomyces* 85E strain was refreshed in the tryptone soya broth medium at 37 ° C. By dispersing new culture spores onto sterile plates with little ISP4 media, the bacterial lawn was created. The compound was loaded onto sterile 5 mm filter paper discs, with 20 μg each disc. After that, the impregnated paper discs were placed on the plates that had been sown with *Streptomyces* 85E. Discs injected with DMSO were utilized as the negative controls. Following a 5–7 days incubation period at 37 °C, the plates showed bald and distinct zones of inhibition surrounding the discs injected with samples and controls.

Antioxidant assay. Antioxidant potential was determined by three different assays.

Free radical scavenging assay. Using 2,2-diphenyl picryl hydrazyl (DPPH) a stable free radical, the antioxidant capabilities of both bare and cefixime-loaded franklinite ($ZnFe_2O_4$) nanostructures were screened. 190 μl of DPPH solution (9.6 mg/100 ml methanol) was added to a fraction of 10 μl from the analyte (1 mg ml^{-1} DMSO) to obtain the ultimate concentration of 50 μg ml^{-1} in the reaction mixture. The mixture was incubated at 37 °C, then the absorbance was measured at 517 nm using a microplate reader after which the percentage of free radical scavenging activity was calculated using the formula,

$$\text{Free radical scavenging activity} = 1 - A_s/A_c \times 100$$

where, A_s and A_c are the absorbances of the sample and negative control, respectively. The assay was performed in triplicate using ascorbic acid as a positive control.

Total reducing power (TRP) determination. To assess the reducing ability of bare green-synthesized as well as cefixime-stabilized franklinite ($ZnFe_2O_4$) nanostructures, the potassium ferricyanide colorimetric method was used. A 100 μl volume of each sample (at a concentration of 1 mg ml^{-1} in DMSO) was mixed with 200 μl of phosphate buffer (0.2 M, pH 6.6 and 250 μl of potassium ferricyanide solution (1% w/v in distilled water)). This mixture was then incubated at 50 °C for 20 minutes in a water bath. Subsequently, 200 μl of trichloroacetic acid (10% w/v in distilled water) was added to each sample before centrifugation at 3000 rpm at 25 °C for 10 minutes. From each

sample, 150 μl of the supernatant was collected and combined with 50 μl of $FeCl_3$ (0.1% w/v in distilled water) in a 96 well plate. The optical density was measured at 630 nm. Ascorbic acid (1 mg ml^{-1} in DMSO) served as a positive control while DMSO acted as a negative control. The reducing power of each sample was expressed in micrograms of ascorbic acid equivalent per milligram of the sample (μg AAE per mg). This procedure was replicated three times using ascorbic acid to calibrate the assay.

Total antioxidant capacity (TAC) determination. The total antioxidant capacity of the green-synthesized bare $ZnFe_2O_4$ nanostructures and those stabilized with cefixime was determined using the phosphomolybdenum method. For this purpose, 900 ml of a TAC solution comprising 0.6 M sulfuric acid, 28 mM sodium phosphate and 4 mM ammonium molybdate was mixed with 100 μl of the sample (prepared at a concentration of 1 mg ml^{-1} in DMSO). DMSO served as the negative control for the experiment. The mixture was then heated in a water bath at 95 °C for 90 minutes. Once cooled, the absorbance of both test and control solutions was measured at 630 nm. The results were expressed in terms of ascorbic acid equivalents, specifically the number of micrograms of ascorbic acid per milligram of the sample dry weight (μg AAE per mg of DW).

Antifungal activity. The antifungal efficacy of the test samples was evaluated through the disc diffusion method on agar. Spore suspension of various fungal species namely *Mucor* species (FCBP-0300), *Aspergillus fumigatus* (FCBP-66), *Aspergillus flavus* (FCBP-0064) and *Aspergillus niger* (FCBP-0198) were prepared in a 0.02% Tween 20 solution. After this, Sabouraud dextrose agar plates were inoculated with 100 μl of each fungal strain, which had been adjusted for turbidity to match the 0.5 McFarland standard. Plates were then treated with discs. Amphotericin B (4 mg ml^{-1}) served as a positive control, DMSO as a negative control and sterile filter paper discs soaked with 5 μl of the samples (concentration of 4 mg ml^{-1} in DMSO) were also applied. Following a 48 hour incubation period at 28 °C the inhibition zones around the sample, positive and negative control discs were measured for their average diameter and recorded.

Results and discussion

Synthesis of franklinite ($ZnFe_2O_4$) nanoparticles

Franklinite ($ZnFe_2O_4$) nanoparticles were obtained using an aqueous extract of *B. asiatica* leaves as a reducing agent, zinc acetate dihydrate and iron sulphate as precursors at room temperature. The easily obtained $ZnFe_2O_4$ nanoparticles were further used as a support to stabilize Cef. Drug-loading efficiency was estimated to be 76%.

X-ray diffraction analysis

The XRD analysis of the synthesized bare and cefixime functionalized $ZnFe_2O_4$ displays a semi-crystalline structure by the presence of three significant peaks shown in Fig. 1A. These peaks at 2θ values of 18.19°, 35.26° and 53.1°, correspond to (111), (311) and (422) reflection planes, respectively. In the

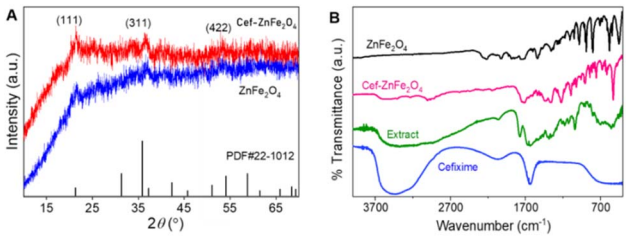

Fig. 1 (A) Comparative XRD patterns of bare and cefixime-functionalized franklinite ($ZnFe_2O_4$) nanostructures. (B) Infrared (FTIR) spectra of cefixime, plant extract, green synthesized bare $ZnFe_2O_4$ nanostructures and cefixime-functionalized franklinite (Cef–$ZnFe_2O_4$) nanostructures.

synthesized material, the peak at 18.19° was slightly shifted and appeared at 21°. The diffraction pattern displays the franklinite structure of the as-synthesized nanoparticles. Diffraction patterns match the standard JCPDS card no. 22-1012. The X-ray diffraction patterns of both bare and cefixime-functionalized franklinite $ZnFe_2O_4$ nanostructures exhibit a higher degree of similarity, particularly in terms of the position of the peaks. A slight difference observed between the two sets of XRD patterns is in the intensity of the peaks. Specifically, the peaks corresponding to the bare franklinite are somewhat more pronounced than those of the drug-loaded nanoparticles. This difference suggests that the inclusion of cefixime into the nanostructures affects the crystallinity, slightly reducing the intensity of diffraction peaks.

Fourier transform infrared (FTIR) analysis

A comparison of FTIR spectra of the plant extract, cefixime, bare and cefixime functionalized $ZnFe_2O_4$ nanostructures indicated their functional groups and possible interactions, as shown in Fig. 1B. Cefixime shows major peaks at 3500–3000 cm^{-1} resembling NH or OH stretching vibrations, along with a carbonyl peak at 1700 cm^{-1}. The extract noticeably displays a broad peak around 3500 cm^{-1} indicative of the OH group, potentially from phenols or alcohols coupled with faint signals at 2000 cm^{-1} along with small peaks in the range of 1500 cm^{-1} to 500 cm^{-1}, which are due to phytochemicals. The primary peaks in the region of 600 cm^{-1} 450 cm^{-1} are indicative of metal–oxygen bonds typically for metal oxides. Cefixime-functionalized $ZnFe_2O_4$ nanostructure interestingly has a spectrum that combines characteristics from the two compounds, a faint peak at 3000 cm^{-1} that resembles both OH or NH groups, a peak at 1700 cm^{-1} that represents a signal from the extract properties, and peaks at 600–450 cm^{-1} that resembles metal–oxygen bonds.

Cefixime shows a sharp carbonyl peak at 1700 cm^{-1} but the noticeable non-uniformity of this peak in the FTIR spectrum of Cef–$ZnFe_2O_4$ shows strong interactions between the cefixime and franklinite surface. This change is likely caused by the carbonyl groups in cefixime binding tightly to the Zn^{2+} and Fe^{3+} ions on the franklinite surface, changing the vibrational characteristics of the C=O bond. Additionally, the hydrogen bonding between cefixime and franklinite weakens the peak of

carbonyl. Similarly, functionalization with nanostructures may induce slight conformational changes in the cefixime molecule, altering the orientation of the carbonyl group and further affecting its vibrational behavior. These combined effects lead to a significant change in the appearance of the peak, highlighting the profound interactions between cefixime and the franklinite nanostructures.

Energy dispersive X-ray spectroscopy (EDX) analysis

EDX spectra shown in Fig. 2A displays remarkable peaks corresponding to iron, zinc and oxygen compatible with the elemental composition expected for $ZnFe_2O_4$. Peak corresponding to zinc is weaker than those for iron, meaning that there is a less percentage of zinc as compared to iron. EDX spectra helped to confirm that zinc is also a part of the material, along with iron. Similarly, EDX spectra (B) of Cef–$ZnFe_2O_4$ Nanostructures exhibit notable peaks corresponding to iron, zinc, oxygen, nitrogen, carbon and sulphur consistent with the expected elements present in both cefixime and franklinite. The franklinite composition was further confirmed using ICP-OES analysis and the atomic ratio of Zn and Fe are in complete agreement with $ZnFe_2O_4$.

UV-visible analysis

Fig. 3 reveals a distinct absorption behavior for plant extract, cefixime, and franklinite ($ZnFe_2O_4$) nanostructures (bare as well as cefixime-loaded). The UV-visible spectrum of *B. asiatica* leaf extract displays a unique range between 250 and 400 nm, which suggests the presence of a complex mixture of phytochemicals. The cefixime spectrum shows specific absorption peaks at 300 nm and a weaker one at 280 nm indicating significant light absorption by certain functional groups. The bare $ZnFe_2O_4$ nanostructures exhibit minimal UV-visible absorbance near 300 nm, indicating the presence of both metal oxides. When cefixime is loaded onto $ZnFe_2O_4$ nanostructures, the spectrum reflects both cefixime and franklinite. Absorption at 280 nm signifies the presence of cefixime within the franklinite nanostructures while a slightly broadened peak around 300 nm hints at potential interaction between cefixime and $ZnFe_2O_4$.

The functional groups such as –COOH and $-NH_2$ in cefixime interact electrostatically with Zn^{2+} and Fe^{3+} ions on the surface of franklinite. These groups may also form hydrogen bonds with hydroxyl groups on the surface of nanostructures, changing the surface environment and affecting UV absorption. Additionally, donor atoms such as nitrogen and oxygen in cefixime can coordinate with the metal ions on the franklinite's surface and weak van der Waals forces between cefixime molecules and the nanostructures further contribute towards the broadening of the peak. These results are consistent with the earlier findings[41] related to doxorubicin-conjugated iron oxide nanoparticles for biomedical applications.

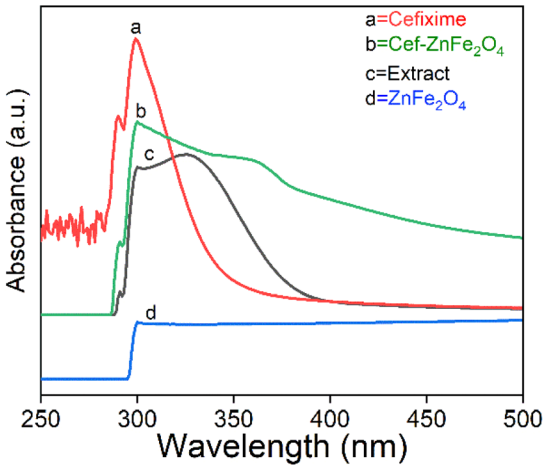

Fig. 3 UV-visible spectroscopy analysis of plant extract, cefixime, franklinite ($ZnFe_2O_4$) and cefixime-loaded franklinite (Cef–$ZnFe_2O_4$).

Electron microscopy analysis

Transmission electron microscopy. Scanning electron microscopy image reveals that the green-synthesized bare franklinite has spherical structures (Fig. 4A). The size of these

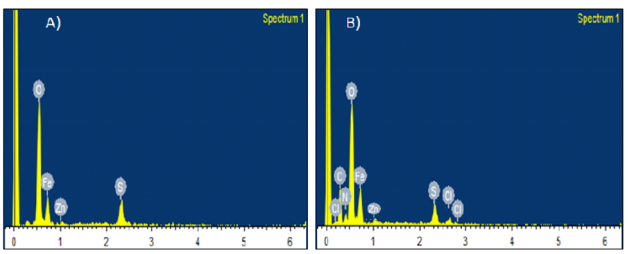

Fig. 2 (A) Energy dispersive X-ray (EDX) spectroscopy analysis of bare $ZnFe_2O_4$ nanostructures. (B) Cefixime-loaded $ZnFe_2O_4$ nanostructures highlighting the differences in elemental makeup due to cefixime incorporation.

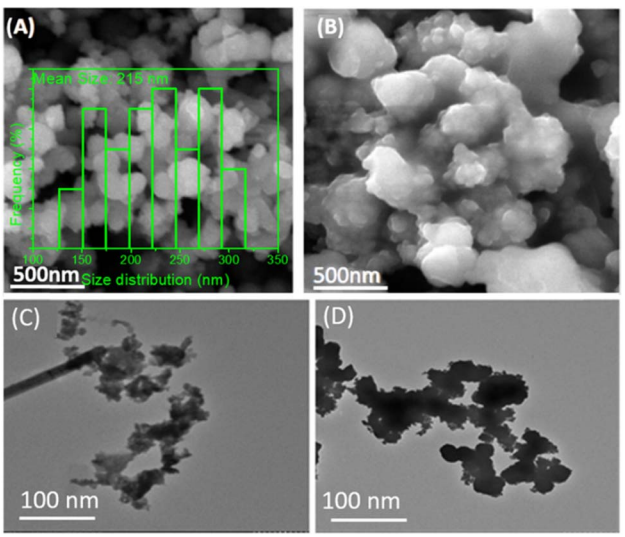

Fig. 4 (A) SEM image and (inset is the size distribution histogram of the particles) (C) TEM image of franklinite ($ZnFe_2O_4$) nanostructures before cefixime loading. (B) SEM image and (D) TEM image of franklinite ($ZnFe_2O_4$) nanostructures after cefixime loading.

spherical particles was measured using nanomeasure and the estimated mean size was 215 nm. The already reported green-synthesized franklinite nanoparticles have a size of about 18.5 nm[42] and 114 nm.[43] Franklinite nanoparticles synthesized using a traditional synthetic approach have an average size of 360 nm[44] and 32.6 nm.[45] The size of currently green-synthesized franklinite nanostructures is smaller and thus better than that of previously reported nanoparticles. However, there are few reports in which the particle size is much smaller than franklinite nanostructures (spheres) reported here[42,45] but these spheres are thought to be secondary structures that are formed by aggregation of sheet-like structures as evidenced from the TEM image. TEM images of bare franklinite shown in Fig. 4C revealed the internal structure of spheres showing that these are actually composed of a collection of sheet-like structures. The SEM image shown in Fig. 4B shows that the addition of cefixime makes the spheres to hold even more tightly together leading to an increase in the apparent diameter, which can be further evidenced from the TEM image (Fig. 4D). A more aggregated structure can be seen in TEM image.

Solubility measurements

Increased temperature enhances the solubility of cefixime-functionalized franklinite ($ZnFe_2O_4$) nanostructures, which could be beneficial for increasing the release rate of therapeutic agents. The solubility of Cef–$ZnFe_2O_4$ nanostructures decreases as the pH increases from 1.2 to 7.4. This trend is consistent at both 25 °C and 37 °C, indicating higher solubility in acidic conditions compared to neutral conditions. This behavior is particularly relevant for therapeutic applications of Cef–$ZnFe_2O_4$ nanostructures in body areas with acidic pH (Table 1).

In vitro bioavailability evaluation

In vitro dissolution testing is an important step in the development of nanoformulation used for therapeutic purposes, particularly in assessing their potential bioavailability. Fig. 5 shows that cefixime-functionalized franklinite (Cef–$ZnFe_2O_4$) indicates a significantly faster release rate reaching 100% release by 120 minutes compared to only 75% for the raw cefixime. These results suggest that the Cef–$ZnFe_2O_4$ nanostructures could potentially enhance the bioavailability of cefixime allowing for faster and more complete absorption in a physiological environment.

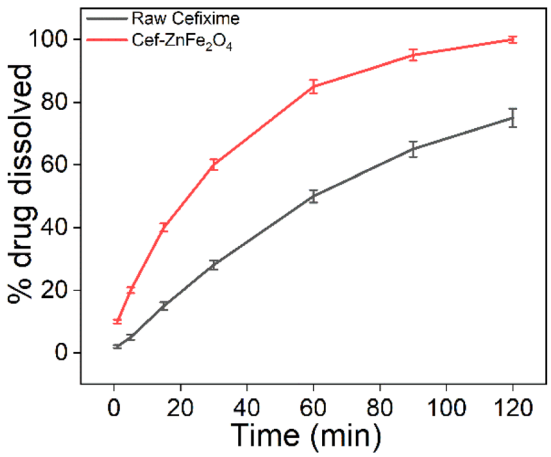

Fig. 5 Comparative dissolution rates of raw cefixime and cefixime loaded franklinite (Cef–$ZnFe_2O_4$) over time. The figure illustrates the enhanced dissolution rate compared to that of raw cefixime, indicating improved *in vitro* bioavailability.

In vitro biocompatibility evaluation

Hemolytic assay. Before using nanoparticles in biomedical applications it is essential to assess their biocompatibility. Many bioactive molecules can cause toxic issues such as hemolysis characterized by the breakdown of human red blood cells leading to the release of hemoglobin. The presence of free hemoglobin in the plasma can damage essential organs including the heart, kidneys and liver.[40] Thus, hemolytic assay is a key aspect of biological research; scientific progress and medical discoveries determine whether a sample is biocompatible with red blood cells or not. According to the American Society for Testing Materials standards for biocompatibility, materials that induce less than 2% hemolysis are known as hemocompatible. Those that cause 2–5% hemolysis are regarded as mildly hemolytic while materials causing more than 5% hemolysis are considered as hemolytic.[46]

In the current research, the hemocompatibility of green-synthesized cefixime-loaded $ZnFe_2O_4$ was evaluated compared to its bare counterpart using human red blood cells at four different concentrations (12.5–100 μg ml^{-1}). Fig. 6A shows that even at maximum concentration, the percentage of hemolysis is very low for $ZnFe_2O_4$ (both bare and cefixime loaded) as compared to the positive control. Fig. 6B shows that the decreasing concentration decreases the hemolytic percentage for Cef–$ZnFe_2O_4$ as well as its counterparts (bare composite and

Table 1 Solubility variations of Cef–$ZnFe_2O_4$ across different temperatures (25 °C and 37 °C) and pH (1.2, 4.5 and 7.4)

pH	Temp. (°C)	S1 (mg l^{-1})	S2 (mg l^{-1})	S3 (mg l^{-1})	Mean ± SD (mg l^{-1})
1.2	25	55.2	50	53	52.73 ± 2.03
1.2	37	62	63	62.8	62.60 ± 0.41
4.5	25	49.7	51	50.5	50.40 ± 0.66
4.5	37	52.3	55	53.8	53.70 ± 1.35
7.4	25	35.1	36	35.5	35.53 ± 0.45
7.4	37	43	45.3	44.2	44.17 ± 1.15

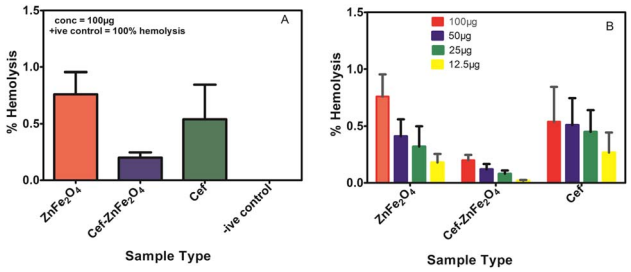

Fig. 6 (A) Comparative analysis of the hemolytic activity induced by cefixime-loaded $ZnFe_2O_4$ nanostructure to its counterparts as well as positive and negative control at maximum concentration. (B) Effect of concentration on % hemolysis of Cef–$ZnFe_2O_4$ and its counterparts.

cefixime). All four concentrations of the synthesized bare and cefixime-loaded nanostructures show their good hemocompatibility. Remarkably, even at a maximum concentration of 100 µg ml^{-1}, as-synthesized Cef–$ZnFe_2O_4$ nanostructures exhibited 0.49% of total hemolytic activity and there was no destruction of red blood cells. From the study's outcome, as-synthesized Cef–$ZnFe_2O_4$ nanostructures are safest to use even at higher concentrations and they might be employed for the therapeutic purpose.

Protein kinase inhibition assay. The protein kinase inhibition approach is important in cancer research due to the fact that these enzymes are involved in the phosphorylation of serine–threonine and tyrosine amino acids. These processes include cellular differentiation, cell proliferation, apoptosis and metabolism. Deregulation of phosphorylation at these amino acid residues by PK enzymes can contribute to tumor growth, which is frequently caused by genetic changes that lead to cancer.[47] To assess the PK inhibition potential of pure as well as cefixime-loaded franklinite aerial hyphae of *Streptomyces* 85E was used. The results for the inhibition of phosphorylation and resultant production of spores and mycelium were assessed in the form of bald and clear inhibition zones (mm) at a sample concentration of 20 µg ml^{-1}. The effective suppression of mycelium development in the test sample was marked by a bald region while a clear region demonstrated the death of a bacterial strain and the toxic effects of the sample. Surfactin-B taken as positive control shows robust inhibition. Among the tested samples Cef–$ZnFe_2O_4$ nanostructures showed significant inhibition with a clear zone (11 mm). This observation suggests that the incorporation of cefixime onto $ZnFe_2O_4$ nanostructures enhances its ability to inhibit protein kinase as compared to its bare counterpart, which shows a bald zone of 11 mm, indicating moderate PK inhibition. These findings suggest the promising potential of Cef–$ZnFe_2O_4$ as a potent kinase inhibitor (Table 2).

Antioxidant activity. The antioxidant potential of bare and cefixime-loaded $ZnFe_2O_4$ nanostructures was assessed using the free radical scavenging assay (DPPH), total antioxidant capacity (TAC), and total reducing power (TRP) assay. The antioxidant potential was recorded using ascorbic acid as a positive control and DMSO as a negative control. All of these assays were performed three times, and the recorded values represent their means ± SEM.

Table 2 Protein kinase inhibition induced by $ZnFe_2O_4$ nanostructures (bare as well as cefixime loaded), cefixime, positive and negative control at 20 µg ml^{-1}

Sample type	Bald zone	Clear zone
$ZnFe_2O_4$	11	—
Cef–$ZnFe_2O_4$	—	11
Cefixime	11	8
Surfactin B	22.3	—
DMSO	0	0

DPPH assay measures the free radical scavenging ability of an antioxidant. Fig. 7A shows that the % mean scavenging for Cef–$ZnFe_2O_4$ is 14.3 ± 0.78. This value is higher than its bare counterpart alone (13.7 ± 0.70) and cefixime alone (13.7 ± 0.1). Enhancement though modest suggests that cefixime loading improves the activity of $ZnFe_2O_4$ nanostructures. Total antioxidant capacity was determined using the phosphomolybdenum-based method where antioxidants reduce Mo(VI) to Mo(V) forming a greenish phosphate molybdate complex. Mean AAE µg per mg ± SD values for positive control, cefixime, Cef–$ZnFe_2O_4$ and bare $ZnFe_2O_4$ are 68 ± 0.24, 25.1 ± 0.25, 25.1 ± 0.27 and 12.3 ± 0.42, respectively, as shown in Fig. 7B. The significant difference between the TAC values of Cef–$ZnFe_2O_4$ nanostructures and $ZnFe_2O_4$ highlights that franklinite has its own intrinsic antioxidant capacity and the presence of cefixime enhances this capacity. TAC value of Cef–$ZnFe_2O_4$ is almost identical to cefixime alone indicating that the antioxidant capacity is retained when loaded onto $ZnFe_2O_4$ nanostructures. The total reducing power of all the tested samples was analyzed using the potassium ferricyanide colorimetric method where the sample converts Fe^{+3} to Fe^{+2} indicated by a blue color formation. TRPs of plant-synthesized pure $ZnFe_2O_4$ nanostructures, Cef–$ZnFe_2O_4$ nanostructures, and cefixime, compared to ascorbic acid at 100 µg mg^{-1} as a positive control, were recorded as 29 ± 0.78, 33 ± 0.7, 65 ± 0.76 and 100 ± 0, respectively, as shown in Fig. 7C. These results show that the Cef–$ZnFe_2O_4$ nanostructure has improved the reducing power

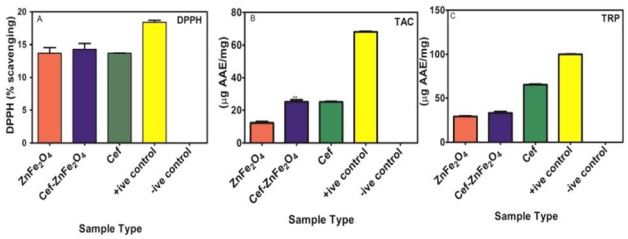

Fig. 7 (A) DPPH radical scavenging activities as percentages, indicating their efficacy in neutralizing free radicals. (B) Mean reducing power determination values ± SEM and (C) mean total antioxidant capacity values ± SEM for Cef–$ZnFe_2O_4$ nanostructures, bare $ZnFe_2O_4$ nanostructures, pure cefixime, ascorbic acid (positive control) and DMSO (negative control) measured in ascorbic acid equivalents AAE µg per mg. Arithmetic variance among groups was evaluated by one-way ANOVA with the Bonferroni test. Key: each bar represents the mean value of three replicates and SEM. Statistical icons: *, **, *** = $p \leq 0.001$.

compared to its bare counterpart indicating a positive effect of cefixime incorporation. However, it remains lower than that of pure cefixime possibly due to the interactions within the nanoparticles matrix that might alter the availability of cefixime active site.

These findings highlight that loading cefixime onto $ZnFe_2O_4$ nanostructures significantly enhances its antioxidant properties. This enhancement makes the cefixime-loaded $ZnFe_2O_4$ nanostructures a promising multifunctional therapeutic agent with both antimicrobial and potent antioxidant properties.

Antifungal assay. The escalating crisis of fungal infections and the growing antifungal resistance highlights the critical need to discover powerful and safe antifungal agents. In this battle, *in vitro* antifungal assays emerge as an indispensable weapon vital for the rigorous screening and evaluation of potential antifungal compounds. Fig. 8 shows the thorough profile of the antifungal activity of $ZnFe_2O_4$ nanostructure, Cef–$ZnFe_2O_4$ nanostructures, cefixime, amphotericin B (positive control) and DMSO (negative control) against four different fungal strains. Comparative antifungal assessments performed in triplicates are presented in the form of inhibition zone (mm) ± SEM error mean, indicating the effectiveness of treatment against each strain. Cefixime shows moderate antifungal activity against all tested fungal strains with inhibition zones ranging from 6–9 mm. Bare $ZnFe_2O_4$ nanostructures exhibited inhibition zones against *A. flavus*, *Mucor* sp and *A. niger* in the range of 7–8 mm showing activity that was almost equal to or slightly better than that of cefixime against these three strains. However, against *A. fumigatus* $ZnFe_2O_4$ nanostructures demonstrated lesser activity with an inhibition zone off only by 2.5 mm compared to cefixime. Cef–$ZnFe_2O_4$ nanostructures demonstrated remarkable efficacy across various fungal strains. The most surprising finding was its outstanding efficacy against *A. flavus* with an inhibition zone of 12 mm surpassing the positive control and all other tested samples. Additionally, the Cef–$ZnFe_2O_4$ nanostructure showed noticeable activity against *Mucor* sp. (11 mm), *A. niger* (10 mm) and *A. fumigatus* (6 mm). These results highlight its greater effectiveness among all the tested samples.

The ability of Cef–$ZnFe_2O_4$ nanostructure to exhibit significant antifungal activity against multiple strains including those that are typically more resistant such as *A. fumigatus* suggests a broad spectrum potential. This efficacy is crucial in clinical settings where infections are often caused by multiple fungal species simultaneously or sequentially.

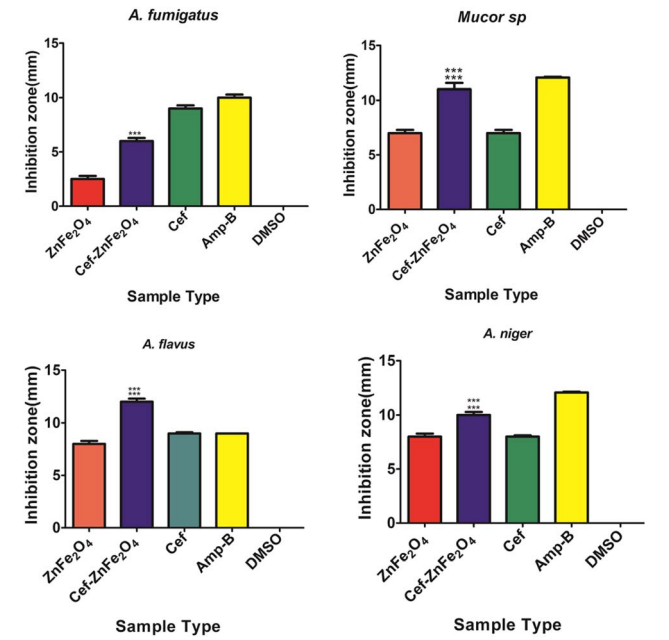

Fig. 8 Antifungal activities comparison: this figure shows the effectiveness of Cef–$ZnFe_2O_4$ nanostructures, bare $ZnFe_2O_4$ nanostructures, cefixime (Cef) and amphotericin B against four fungal species. Results are indicated as mean ± SEM from three replicates. Arithmetic variance among groups was evaluated by one-way ANOVA with the Bonferroni test, which reveals a significant enhancement in antifungal activity of Cef–$ZnFe_2O_4$ nanostructures over independent Cef and $ZnFe_2O_4$ nanostructures ($b = p \leq 0.05$). Key: each bar represents the mean value of three replicates and SEM. Statistical icons: *, **, *** = $p \leq 0.05$.

Conclusions

Franklinite ($ZnFe_2O_4$) nanostructures were synthesized *via* the green method and successfully loaded with cefixime. Drug loading was validated and characterized using FTIR, UV, XRD, SEM, TEM and EDX techniques. *In vitro* hemolytic assay, antifungal, protein kinase and antioxidant activities were investigated. Results indicated that incorporating cefixime onto presynthesized $ZnFe_2O_4$ nanostructures enhances their surface area, significantly improving antifungal, antioxidant and kinase inhibition activities compared to its counterpart. The hemolytic assay demonstrated increased hemocompatibility of cefixime–franklinite. Furthermore, solubility measurements indicated increased solubility at body temperature and in acidic conditions while the dissolution test showed an enhanced dissolution rate suggesting improved *in vitro* bioavailability and enhanced effectiveness in the physiological environment. These findings suggest that the green synthesis of $ZnFe_2O_4$ nanostructures with cefixime loading could offer an effective strategy for enhancing the therapeutic efficacy, safety, bioavailability and solubility of cefixime under physiological conditions.

Data availability

The data can be obtained from corresponding author upon reasonable request.

Author contributions

Amna Munsaf performed experimentation, writing the draft and drawing all the figures and their interpretation. Muhammad Naeem Ahmed designed, conceptualized and supervised the whole project. Aroosa Zafar carried out the biological studies. Bilal Akram and Mahmoud A. A. Ibrahim performed characterization.

Conflicts of interest

The authors declare no competing financial interest.

Acknowledgements

We are thankful to the University of Azad Jammu and Kashmir for financial support.

Notes and references

1 S. Frosyth, P. Penney and G. Rooney, *Int. J. STD AIDS*, 2011, **22**, 296–297.
2 F. Mottaghitalab, M. Farokhi, Y. Fatahi, F. Atyabi and R. Dinarvand, *J. Controlled Release*, 2019, **295**, 250–267.
3 A. Zehra, B. Naqvi, R. Bushra and S. Ali, *Jordan J. Pharm. Sci.*, 2010, **3**, 2.
4 B. S. Schtaz, K. T. Karavokiros, M. A. Taeubel and G. S. Itokazu, *Ann. Pharmacother.*, 1996, **30**, 258–268.
5 V. Weissig, T. Elbayoumi, B. Fluhmann and A. Barton, *Am. J. Pharm. Educ.*, 2021, **85**, 8331.
6 D. W. Schaefer and R. S. Justice, *Macromolecules*, 2007, **40**, 8501–8517.
7 S. Komarneni, *J. Mater. Chem.*, 1992, **2**, 1219–1230.
8 S. K. Kumar and R. Krishnamoorti, *Annu. Rev. Chem. Biomol. Eng.*, 2010, **1**, 37–58.
9 T. Hassan, A. Salam, S. U. Khan, H. Khanzada, M. Wasim, M. Q. Khan and I. S. Kim, *J. Polym. Res.*, 2021, **28**, 36.
10 S. K. Kumar and R. Krishnamoorti, *Annu. Rev. Chem. Biomol. Eng.*, 2010, **1**, 37–58.
11 A. Sood, V. Arora, J. Shah, R. K. Kotnala and T. K. Jain, *Mater. Sci. Eng., C*, 2017, **80**, 274–281.
12 P. D. Mangalgiri, *Bull. Mater. Sci.*, 1999, **22**, 657–664.
13 D. Zablotsky, I. Segal, A. Zablotskaya, M. Maiorov and T. A. Nguyen, *Magnetic Nanoparticle-Based Hybrid Materials*, Woodhead Publishing, 2021, pp. 501–527.
14 C. Pragathiswaran, C. Smitha, H. Barabadi, M. M. Al-Ansari, L. A. Al-Humaid and M. Saravanan, *Inorg. Chem. Commun.*, 2020, **121**, 108210.
15 S. Kumar, M. K. Shukla, A. K. Sharma, G. K. Jayaprakash, R. K. Tonk, D. K. Chellappan, S. K. Singh, K. Dua, F. Ahmed, S. Bhattacharyya and D. Kumar, *MedComm*, 2023, **4**, e253.
16 H. Malhotra, A. Kamboj and R. K. Gautam, *Metal Nanocomposites in Nanotherapeutics for Oxidative Stress-Induced Metabolic Disorders*, CRC Press, 2023, pp. 327–348.
17 M. Pourmadadi, E. Rahmani, A. Shamsabadipur, S. Mahtabian, M. Ahmadi, A. Rahdar and A. M. Diez-Pascual, *Nanomaterials*, 2022, **12**, 3873.
18 L. L. Beecroft and C. K. Ober, *Chem. Mater.*, 1997, **9**, 1302–1317.
19 B. Mishra, S. Varjani, D. C. Agrawal, S. K. Mandal, H. H. Ngo, M. J. Taherzadeh and W. Guo, *Environ. Technol. Innovation*, 2020, **20**, 101063.
20 *Nanocomposites-Advanced Materials for Energy and Environmental Aspects*, ed. M. E. Khan, J. Aslam and C. Verma, Elsevier, 2023.
21 S. J. Owonubi, N. M. Malima and N. Revaprasadu, in *Antibiotic Materials in Healthcare*, Academic Press, 2020, pp. 287–323.
22 L. Gavrila-Florescu, F. Dumitrache, M. Balas, C. T. Fleaca, M. Scarisoreanu, I. P. Morjan and G. Prodan, *Appl. Phys. A: Mater. Sci. Process.*, 2017, **123**, 1–13.
23 M. T. S. Chani, S. B. Khan, M. M. Rahman, T. Kamal and A. M. Asiri, *J. King Saud Univ., Sci.*, 2022, **34**, 101841.
24 H. Kang, S. Mintri, A. V. Menon, H. Y. Lee, H. S. Choi and J. Kim, *Nanoscale*, 2015, **7**, 18848–18862.
25 D. Mishra, J. R. Hubenak and A. B. Mathur, *J. Biomed. Mater. Res., Part A*, 2013, **101**, 3646–3660.
26 S. Lee, H. Park and K. H. Yoo, *Adv. Mater.*, 2010, **22**, 4049–4053.
27 K. Letchford and H. Burt, *Eur. J. Pharm. Biopharm.*, 2007, **65**, 259–269.
28 A. Vonarbourg, C. Passairani, P. Saulnier and J. P. Benoit, *Biomaterials*, 2006, **27**, 4356–4373.
29 A. Goyal, S. Bansal and S. Singhal, *Int. J. Hydrogen Energy*, 2014, **39**, 4895–4908.
30 W. Gac, W. Zawadzki, G. Slowik, M. Greluk and A. Machocki, *J. Therm. Anal. Calorim.*, 2016, **125**, 1205–1215.
31 L. Han, X. Zhou, L. Wan, Y. Deng and S. Zhan, *J. Environ. Chem. Eng.*, 2014, **2**, 123–130.
32 A. Manohar, V. Vijayakanth, S. P. Vattikuti and K. H. Kim, *Mater. Chem. Phys.*, 2022, **286**, 126117.
33 S. Vijayakumar, B. Vaseeharan, B. Malaikozhundan and M. Shobiya, *Biomed. Pharmacother.*, 2016, **84**, 1213–1222.
34 J. R. Peralta-Videa, Y. Huang, J. G. Parsons, L. Zhao, L. Lopez-Moreno, J. A. Hernandez-Viezcas and J. L. Gardea-Torresdey, *Nanotechnol. Environ. Eng.*, 2016, **1**, 1–29.
35 A. N. D. Krupa and R. Vimala, *Mater. Sci. Eng., C*, 2016, **61**, 728–735.
36 F. T. Thema, E. Manikandan, M. S. Dhlamini and M. J. L. Maaza, *Mater. Lett.*, 2015, **161**, 124–127.
37 K. Parveen, V. Banse and L. Ledwani, *AIP Conf. Proc.*, 2016, **1724**(1), 1–7.
38 F. M. Arvanag, A. Bayrami, A. H. Yangjeh and S. R. Poursan, *Mater. Sci. Eng., C*, 2019, **97**, 397–405.
39 V. Ramalingam, P. Muthukumar Sathya, S. Thimmaarayan and H. Mohan, *Life Sci.*, 2022, **309**, 121022.
40 Y. Du, L. Xia, A. Jo, R. M. Davis, P. Bissel, M. F. Ehrich and D. G. I. Kingston, *Bioconjugate Chem.*, 2018, **29**, 420–430.
41 N. Singh, N. Millot, L. Maurizi, G. Lizard and R. Kumar, *ACS Omega*, 2020, **5**, 16165–16175.
42 A. Imraish, T. Abu Thiab, W. Al-Awaida, H. J. Al-Ameer, Y. Bustanji, H. Hammad and A. Al-Hunaiti, *J. Food Biochem.*, 2021, **45**(6), e13730.
43 A. Al-Zabin, T. Abu Thiab, M. Zihlif, A. Al-Hunaiti, H. J. Al-Ameer, W. Al-Awaida and A. Imraish, *Biomed. Rep.*, 2024, **20**(3), 1–9.
44 M. Zhang, F. Zhao, Y. Yang, H. Li, H. Gao, E. Yao and Z. Jiang, *J. Therm. Anal. Calorim.*, 2020, **141**, 1413–1423.
45 H. Wu, Q. Wu, J. Zhang, Q. Gu, W. Guo, S. Rong and X. Jing, *Sci. Rep.*, 2021, **11**(1), 17113.
46 V. M. Gandhi and K. M. Cherian, *Toxicol. In Vitro*, 2000, **14**, 513–516.
47 R. Kannaiyan and D. Mahadevan, *Expert Rev. Anticancer Ther.*, 2018, **18**, 1249–1270.